Magnetic Particle Imaging: A Novel in vivo Imaging Platform for Cancer Detection

Elaine Y. Yu[†], **Mindy Bishop**[†], **Bo Zheng**[†], **R. Matthew Ferguson**[‡], **Amit P. Khandhar**[‡], **Scott J. Kemp**[‡], **Kannan M. Krishnan**[¶], **Patrick W. Goodwill**[§], and **Steven M. Conolly**[†,ǁ]

[†]Department of Bioengineering, University of California, Berkeley, California 94720, United States

[‡]Lodespin Labs LLC, Seattle, Washington 98103, United States

[¶]Department of Materials Science, University of Washington, Seattle, Washington 98195, United States

[§]Magnetic Insight, Inc., Alameda, California 94501, United States

[ǁ]Department of Electrical Engineering and Computer Sciences, University of California, Berkeley, California 94720, United States

Abstract

Cancer remains one of the leading causes of death worldwide. Biomedical imaging plays a crucial role in all phases of cancer management. Physicians often need to choose the ideal diagnostic imaging modality for each clinical presentation based on complex trade-offs between spatial resolution, sensitivity, contrast, access, cost, and safety. Magnetic particle imaging (MPI) is an emerging tracer imaging modality that detects superparamagnetic iron oxide (SPIO) nanoparticle tracer with high image contrast (zero tissue background signal), high sensitivity (200 nM Fe) with linear quantitation and zero signal depth attenuation. MPI is also safe in that it uses safe, in some cases even clinically approved tracers and no ionizing radiation. The superb contrast, sensitivity, safety, and ability to image anywhere in the body lends MPI great promise for cancer imaging. In this study, we show for the first time the use of MPI for *in vivo* cancer imaging with systemic tracer administration. Here, long circulating MPI-tailored SPIOs were created and administered intravenously in tumor bearing rats. The tumor was highlighted with tumor-to-background ratio of up to 50. The nanoparticle dynamics in the tumor was also well appreciated, with initial wash-in on the tumor rim, peak uptake at 6 hours, and eventual clearance beyond 48 hours. Lastly, we demonstrate the quantitative nature of MPI through compartmental fitting *in vivo*.

Keywords

Magnetic Particle Imaging; medical imaging; nanoparticles; cancer imaging

Biomedical imaging plays a key role in every phase of clinical cancer management, starting from initial screening through diagnosis, staging, treatment planning, and treatment monitoring.[1] The defining challenge in all cancer imaging is to robustly distinguish tumor

Correspondence to: Steven M. Conolly.

from healthy tissue. Current anatomical imaging techniques such as X-ray, X-ray computed tomography (CT), ultrasound, and MRI are very useful for detecting tissue architecture changes that generally accompany cancer, but the native contrast of tumors may not differ sufficiently from healthy tissues for a confident diagnosis, especially for metastatic or diffuse tumors.[2] Hence, exogenous contrast agents such as Iodine (for X-ray CT), Gadolinium (for MRI), microbules (Ultrasound) and ^{18}FDG or ^{99m}Tc (for PET and SPECT) are often administered to highlight crucial physiologic contrast between normal and cancerous tissue for more precise screening, diagnosis, staging, and treatment planning. These agents are all injected intravenously but their method of highlighting tumors differs considerably. Nuclear medicine uses metabolic tracer reporters, which preferentially accumulate in cancer due to the enhanced metabolic activity of tumors. Iodine and Gadolinium-based contrast agents distribute throughout the extracellular space and are cleared rapidly by glomerular filtration. This simple process has been exploited extensively in radiology to indirectly highlight tumors.[2] Nano-sized agents are known to be advantageous over conventional low molecular weight agents for several reasons. Nano-sized agents that are carefully designed to be large enough to escape excretion by the kidney, yet small enough to prevent immediate clearance from the reticuloendothelial system (RES), are able to circulate in the blood for extended periods of time. In some tumors, leaky vasculature permits these long-circulating nano-sized agents to preferentially leak into tumor tissue where they are then retained in the tumor bed due to reduced lymphatic drainage. This process is known as the enhanced permeability and retention (EPR) effect.[3–5]

Physicians choose the ideal diagnostic imaging modality for each clinical presentation based on complex trade-offs between spatial resolution, sensitivity, contrast, access, cost, and safety. X-Ray systems, including CT, have mmol/kg sensitivity to iodinated contrast.[6] Gd-MRI T1 agents show *positive contrast*, with relaxivity of 5 Hz/mM,[7] showing roughly 200 micromolar gadolinium concentration sensitivity. Superparamagnetic iron oxide (SPIO) nanoparticles, on the other hand, have a much larger effect on the MRI signal with the trade-off that they typically show T2* "negative contrast", which is difficult to distinguish from tissues such as bone, tendon and the lung. PET and nuclear medicine has exquisite sensitivity, ranging from nmol/kg to pmol/kg.[6] However, preparation of radiopharmaceuticals is expensive and requires cumbersome "hot chemistry". Moreover, nuclear medicine relies heavily on ^{99m}Tc (6-hour half-life) and ^{18}FDG (2-hour half-life), which fundamentally limits the duration of pathophysiology one can monitor with these radionuclides. Longer half-life tracers are available for monitoring slowly evolving pathophysiology (e.g., Indium 111 2.8-day half-life), but the longer half-life involves either greater net dose to the patient or weaker SNR. Indeed, X-ray, CT, and nuclear medicine expose patients to ionizing radiation and contrast media used for MRI and CT can be harmful to patients, especially patients with Chronic Kidney Disease (CKD). Due to the risks, and in many cases low diagnostic benefit due to insufficient contrast as well as high cost, most existing imaging techniques are carefully evaluated before incorporation into the cancer management workflow.

Magnetic Particle Imaging (MPI),[8–11] introduced by Philips Research in 2005, is a tracer imaging modality that directly measures the location and concentration of SPIO nanoparticles *in vivo*. MPI images the SPIO electronic moment, which is 22-million times

more intense than **nuclear** MRI moments.[12] During signal generation, the application of a time-varying homogeneous excitation field causes SPIOs to instantaneously flip, thereby inducing a signal in the receive coil. To localize this signal, a field-free point (FFP) is created with a strong magnetic gradient. All particles outside the FFP are saturated, and only the particles at the FFP are able to flip when an addition of time-varying homogeneous excitation field is applied to the imaging field of view (FOV). The FFP is then rastered throughout the FOV, and the signal detected is assigned to an image location corresponding to the instantaneous location of the FFP.[13] This imaging process is illustrated in Figure 1(a). Note that this is just one of the many possible trajectories suited for FFP MPI.[10,14]

MPI is linearly quantitative, as shown in Figure 1(c). Although an ensemble of particles responds nonlinearly to an applied magnetic field, the voltage induced in the receiver coil is directly proportional to the amount of iron present at the FFP. MPI is also highly sensitive, detecting nanograms of iron (or 200 labeled cells) per voxel.[15,16] The current resolution with MPI-tailored SPIOs[17,18] is approximately 1 mm, but may improve to better than 300 μm resolution with optimized nanoparticles, improved imaging hardware, and pulse sequences.[19] In addition, due to the low frequency magnetic fields used in MPI, there is zero signal depth attenuation from biological tissue, and there is zero signal from the tissue itself – only particle signal is visualized. This high contrast is highly enabling, as it allows clear visualization of tissue perfusion and targeting processes. In addition to producing no ionizing radiation, iron-oxide tracers are also safe, some of which are clinically approved as MRI contrast agents.[20,21] Hence, it is safe to repeat serial scans on an animal or human. At present, no human MPI scanner has been developed, but the small animal MPI scanners are comparable in complexity to MRI scanners, so clinical translation should be feasible. The superb contrast, sensitivity, safety, and ability to image anywhere in the body gives MPI great promise for cancer imaging.

In this study, we show for the first time the use of MPI for *in vivo* cancer imaging. We used the first MPI-tailored particles which exhibit superior resolution, circulation time, and SNR over existing MPI tracers, which was invaluable for this study. We intravenously administered the SPIOs in tumor bearing rats and monitored the dynamic *in vivo* distribution of SPIOs using MPI over a period of 6 days. Due to the high contrast inherent to MPI, we captured clear images of the nanoparticle dynamics in the tumor and measured vascular wash-in, accumulation due to Enhanced Permeability Retention (EPR) effect, and subsequent clearance. The high contrast images also enabled quantitative analysis on tracer dynamics.

A custom-built FFP MPI imager was used for this study, the construction of which is previously described.[22,23] The 3D MPI scanner has a drive field frequency of 20.225 kHz and an excitation strength of 40 mTpp. The FFP is created with NdFeB permanent magnets (gradient of $7 \times 3.5 \times 3.5$ T/m) and shifted with electromagnets following a trajectory through the field of view. All images were reconstructed using x-space MPI reconstruction algorithm.[9,13,24] Each *z* frame, as shown in Figure 1(a), covers a FOV of $4 \times 4 \times 0.166$ cm, and is separated into 48 lines in the *x* direction. The *z* frames (5.76 seconds per frame) are acquired at 2 mm increments, allowing for the stitching required in x-space MPI reconstruction.

MPI-tailored SPIO tracer (LS-008, LodeSpin Labs) was synthesized[11,25] to achieve optimal resolution and blood circulation half-life. The iron oxide nanoparticles were synthesized by thermolysis of iron III oleate in 1-octadecene, with subsequent oxidation to achieve desired magnetic behavior using a mix of 1 % oxygen in argon.[26] Biocompatible poly(maleic anhydride alt-1-octadecene) (PMAO)-PEG(20k) coatings were prepared by attaching 20 kDa Methoxy-PEG-amine (JenKem USA) to PMAO (Sigma) (30–50 kDa).[25] The iron-oxide nanoparticles were then coated with amphiphilic polymer coating and dispersed in PBS buffer for characterization and animal studies. Tracer was injected in the tail vein of female CD-1 mice (7 weeks old, n = 9) at 5 mg Fe/kg dose. Tracer blood half-life was then characterized according to a previously published method[18] based on *ex vivo* Magnetic Particle Spectrometry (MPS) measurements of blood drawn at various time points during circulation. Using MPS, the magnetization response of SPIOs in an AC field can be measured, allowing quantitation of SPIO concentration in the collected blood samples. These animal procedures were approved by the IACUC at University of Washington.

Bright field TEM and Selected Area Electron Diffraction (SAED) were performed at 200 keV to characterize nanoparticle morphology and size, and crystalline phase, respectively, as shown in Figure 2(a). For size determination, n=1,960 particles were analyzed from 4 different images at 195k magnification. Inverse spinel (magnetite/maghemite) phase structure was confirmed by SAED. Blood half-life of the tracer was determined by fitting MPS signal data to a first-order pharmacokinetic elimination profile (single exponential decay); the half-life ($t_{1/2}$) was 105 ± 10 minutes ($R^2 = 0.99$), as shown in Figure 2(b). Hydrodynamic size of the coated nanoparticles was measured in PBS using Dynamic Light Scattering (DLS, Malvern ZetaSizer Nano ZS); the Z-average diameter was 90.7 nm (Figure 2(c)). Magnetic properties were measured by VSM (Lakeshore, Figure 2(d)) and by a custom-built magnetic particle spectrometer MPS (data not shown). Magnetic size was 26.3 nm, determined by fitting of M(H) data to a Langevin function (following Chantrell's method[27]).

We evaluated the potential of *in vivo* MPI cancer imaging in 7 athymic nude rats bearing xenograft breast tumors. The animals were prepared by subcutaneous implantation of 7 million MDA-MB-231-luc cells. The presence of the tumor was confirmed with optional bioluminescence imaging (IVIS Lumina) after intraperitoneal injection of luciferin substrate as shown in Figure 1(d). MPI-tailored long circulating SPIO tracer (LS-008) was administered systemically through the tail vein 4 weeks post tumor implantation. The rats were separated into 3 groups, Groups A, B, and C. In Group A (n = 3), the tumors were implanted in the left lower mammary fat pad and LS-008 was intravenously administered at a dose of 15 mg/kg. In Group B (n = 3), the tumors were implanted at the right lower flank and LS-008 was intravenously administered at a dose of 5 mg/kg. In Group C (n = 1), control animal had no tumor and was injected with LS-008 at a dose of 15 mg/kg. For reference, the ranges of dosages reported for human and small animal imaging studies in literature are 0.5 – 7.3 mg Fe/kg and 0.0145 – 56 mg Fe/kg, respectively.[20,28,29] MPI scans were then acquired at multiple time points up to 6 days post injection. Post-mortem CT scans were acquired on a RS9-80 Micro CT scanner (GE) with 17-minute acquisition time and 93 μm isotropic resolution for anatomical reference. These animal procedures were

conducted in accordance to the National Research Council Guide for the Care and Use of Laboratory Animals and approved by the UC Berkeley Animal Care and Use Committee.

The tracer biodistribution through time in Group A rats (high dose, 15 mg/kg) is shown in Figure 3. The MPI images with a field of view (FOV) of $4 \times 4 \times 8.5$ cm and acquisition time of 5 minutes were captured for these rats. For Group A rats, the MPI imaging volume captured only the lower abdomen where the tumor was present, along with and part of the liver and spleen. The images in Figure 3 are cropped to a FOV of $4 \times 4 \times 5.8$ cm to focus on particle dynamics in the tumor as clearly visualized with MPI. The initial vascular wash-in is characterized by the rim enhancement of the tumor. Consistent with the enhanced permeability and retention (EPR) effect reported in literature, nanoparticles preferentially accumulate in tumors due to their abnormally leaky vasculature.[3,5] By 96 hours, the particles have cleared. The dynamics of EPR effect is clearly captured with MPI, with a tumor-to-background ratio of up to 50 at 6 hours post injection. Due to the high contrast inherent to MPI and long tracer half-life, tracer present in the tumor was detectable as long as 6 days post injection.

The tracer biodistribution through time in Group B rats (low dose, 5 mg/kg) is shown in Figure 4. Here, we measured the full body biodistribution with a FOV of $4 \times 4 \times 14.5$ cm with an acquisition time of 9 minutes. Whole body maximum intensity projection (MIP) of the 3D MPI image volumes were coregistered with CT skeletal reference. As is apparent in Figure 4, the injected LS-008 particles are first distributed uniformly in the intravascular system, yielding a blood volume image. Organs with larger blood volume such as the heart and lungs are therefore distinguishable. Although specific biodistribution and clearance parameters depend on particle properties such as surface characteristics, shape, and size, iron oxide nanoparticles are primarily cleared from the blood by the RES.[30] Our MPI measurements confirm this: intravascular signal decreases gradually with time, while signal in the liver and spleen increase over time. Simultaneously, the contrast and sensitivity inherent to MPI allows for the tumor to be clearly visible through time. Since the tumors in this study are subcutaneous xenografts, the tumors are prone to slight shifts while being loaded into the scanner for each time point. This is reflected in the slight changes in tumor position in the MPI scans over time.

Due to the quantitative nature of MPI with zero depth attenuation, we were able to not only noninvasively track the biodistribution through time, but also model the tracer dynamics in a two compartment model. Group A and B biodistribution and compartmental fitting are shown in Figure 5(a) and (b), respectively. For each 3D MPI volume, the MPI signal was first calibrated to to a known concentration based on the calibration curve shown in Figure 1(c). Regions of interest (ROI) were identified for each organ in which the concentration is averaged. For the blood, the ROI was drawn in the left femoral artery. For two-compartmental fitting, the estimated blood pool volume of the blood pool based on weight of the animal and measured size of the tumor were used for one representative rat in each group.

Group A was injected with 3-fold the dose of Group B, and the measured concentration of tracer in blood (derived directly from *in vivo* MPI signal) differed by 3-fold, as apparent in

Figure 5(a) and (b). This gives us confidence in the quantitative nature of MPI for SPIOs *in vivo*. Tracer blood circulation half-life was calculated to be 4.25 ± 0.28 hours for group A (high dose) and 3.65 ± 0.71 hours for group B (low dose). This dose dependency of iron-oxide blood half-life due to progressive saturation of the macrophage uptake in macrophage-rich organs is a well-known phenomenon that has been demonstrated for various particle systems.[31] This could explain the relatively larger accumulation of particles in Group A tumors. Although EPR effect is known to passively target tumors, there is also a large variability of vascular development across tumor types and sizes. Therefore, it is well-known that EPR effect does not manifest in all tumors. We observed this variability in enhancement at later time points in our experiment as shown in the bottom panels of Figure 5(a) and (b). However, the initial vascular wash-in rim enhancement was readily apparent in all animals.

To confirm the presence of tracer, organs were dissected at the end point and imaged with MPI as shown in Figure 5(c). Presence of SPIO signal was observed in liver, spleen, as well as the tumor 2 days post injection. In one case, the rat was sacrificed 6 days post injection, and SPIO signal was still observed in the tumor with a tumor to muscle signal ratio as high as 4.98.

This is the first demonstration of cancer detection with MPI through passive targeting – perfusion and EPR effect. Another study has shown MPI of direct SPIO injections into tumor.[32] Indeed, EPR effect is not without its limitations. There is significant heterogeneity within and between tumor types – different types of tumors have different pore dimensions in the vasculature and the maximum pore size changes with the location for a given type of tumor. Most studies demonstrating nanotechnology platforms that effectively exploit the EPR effect have been done in implanted tumors, with limited data on metastatic lesions.[33] Therefore, continued development is required before nanoparticles can be fully realized in clinical use for cancer. Our current SPIO tracer has around 2 hour circulation half-life in mice and around 3.5 hour half-life in rats, which may be adequate for cardiovascular imaging and for certain cancer studies as shown here. However, it may be the case that extended circulation time is attractive for improving the contrast of certain pathophysiology. For these applications, nanoparticles can be encapsulated in PEGylated PRINT nanoparticles with circulation half-life of 19.5 hours[34] or in red blood cells with tracer life span in the mice bloodstream prolonged to 12 days.[35]

To improve the specificity of cancer imaging, researchers have bound the most common contrast agents and nuclear medicine tracers to moieties that are thought to home to tumor biomarkers, including peptides,[36] antibodies,[37] and cells.[38] These are all targeting strategies that can be realized with MPI. In particular, MPI is capable of *in vivo* non-invasive cell tracking with MPI with 200-cell sensitivity.[15,16,39,40] Additionally, the use of relaxation and aggregation-based SPIO contrast mechanisms have been demonstrated.[41,42] This may enable *in vivo* sensing of tumor micro-environment factors such as viscocity and pH to provide additional contrast.

There is a growing field of magnetic nanomaterial development for targeted drug delivery[43] and hyperthermia,[44] many currently designed to be used as contrast agents in MRI.[45] Due to the inherently lower sensitivity and negative contrast of SPIOs in MRI, rim enhancement of

the tumor as we have observed in this study with MPI is difficult to see with MRI, even with dosages as high as 27.92 mg Fe/kg. Tumor enhancement is seen at later time points in the center of the tumor,[46] similar to what we have also observed in our study. There have been several promising demonstrations of MPI guided magnetic hyperthermia.[32,47] In addition, we are in the early stages of demonstrating the potential for localized magnetic hyperthermia with simultaneous imaging using the existing gradient field in MPI.[48] It is evident that many cancer targeting strategies for magnetic nanoparticles are already widely investigated. MPI, with its superb sensitivity and contrast, is uniquely poised to harness this existing work to even more efficiently target and image cancer. Indeed, MPI can also serve as a powerful tool for researchers developing targeted magnetic nanoparticles, and may ultimately enable safe and high contrast cancer detection in the clinic.

Acknowledgments

References

1. Hillman BJ. J Clin Oncol. 2006; 24:3223–3224. [PubMed: 16829645]

2. Frangioni JV. J Clin Oncol. 2008; 26:4012–4021. [PubMed: 18711192]

3. Kobayashi H, Watanabe R, Choyke PL. Theranostics. 2013; 4:81–89. [PubMed: 24396516]

4. Maeda H. Adv Enzyme Regul. 2000; 41:189–207.

5. Maeda H, Nakamura H, Fang J. Adv Drug Delivery Rev. 2013; 65:71–79.

6. Fass L. Mol Oncol. 2008; 2:115–152. [PubMed: 19383333]

7. Caravan P, Ellison JJ, McMurry TJ, Lauffer RB. Chem Rev. 1999; 99:2293–2352. [PubMed: 11749483]

8. Gleich B, Weizenecker J. Nature. 2005; 435:1214–1217. [PubMed: 15988521]

9. Goodwill PW, Conolly SM. IEEE Trans Med Imag. 2010; 29:1851–1859.

10. Weizenecker J, Gleich B, Rahmer J, Dahnke H, Borgert J. Phys Med Biol. 2009; 54:L1–L10. [PubMed: 19204385]

11. Khandhar AP, Keselman P, Kemp SJ, Ferguson RM, Goodwill PW, Conolly SM, Krishnan KM. Nanoscale. 2017; 9:1299–1306. [PubMed: 28059427]

12. Schenck JF. Med Phys. 1996; 23:815–850. [PubMed: 8798169]

13. Goodwill PW, Conolly SM. IEEE Trans Med Imag. 2011; 30:1581–1590.

14. Knopp T, Biederer S, Sattel T, Weizenecker J, Gleich B, Borgert J, Buzug TM. Phys Med Biol. 2008; 54:385. [PubMed: 19098358]

15. Zheng B, von See MP, Yu E, Gunel B, Lu K, Vazin T, Schaffer DV, Goodwill PW, Conolly SM. Theranostics. 2016; 6:291–301. [PubMed: 26909106]

16. Zheng B, Vazin T, Goodwill PW, Conway A, Verma A, Ulku Saritas E, Schaffer D, Conolly SM. Sci Rep. 2015; 5:14055. [PubMed: 26358296]

17. Ferguson RM, Khandhar AP, Kemp SJ, Arami H, Saritas EU, Croft LR, Konkle J, Goodwill PW, Halkola A, Rahmer J, Borgert J, Conolly SM, Krishnan KM. IEEE Trans Med Imag. 2015; 34:1077–1084.

18. Khandhar AP, Ferguson RM, Arami H, Krishnan KM. Biomaterials. 2013; 34:3837–3845. [PubMed: 23434348]

19. Yu, E., Zheng, B., Tay, ZW., Keselman, P., Zhou, X., Orendorff, R., Hensley, DW., Ferguson, RM., Khandhar, AP., Kemp, SJ., Krishnan, KM., Goodwill, PW., Conolly, SM. World Molecular

Imaging Congress. 2016. In vivo Projection Imaging and 3D Computed Tomography Magnetic Particle Imaging with a High Resolution 6 T/m Field Free Line Electromagnet.

20. Wang YXJ. Quant Imaging Med Surg. 2011; 1:35–40. [PubMed: 23256052]

21. Lu M, Cohen MH, Rieves D, Pazdur R. Am J Hematol. 2010; 85(5):315–319. [PubMed: 20201089]

22. Saritas EU, Goodwill PW, Croft LR, Konkle JJ, Lu K, Zheng B, Conolly SM. J Magn Reson. 2013; 229:116–126. [PubMed: 23305842]

23. Goodwill, PW., Croft, LR., Konkle, JJ., Lu, K., Saritas, EU., Zheng, B., Conolly, SM. A 7 T/M 3D X-space MPI mouse and rat scanner. 2013 International Workshop on Magnetic Particle Imaging (IWMPI); 2013; p. 1-1.

24. Lu K, Goodwill P, Saritas E, Zheng B, Conolly S. IEEE Trans Med Imag. 2013:1–11.

25. Khandhar AP, Ferguson RM, Arami H, Kemp SJ, Krishnan KM. IEEE Trans Magn. 2015; 51

26. Kemp SJ, Ferguson RM, Khandhar AP, Krishnan KM. RSC Adv. 2016; 6:77452–77464.

27. Chantrell R, Popplewell J, Charles S. IEEE Trans Magn. 1978; 14:975–977.

28. Arami H, Khandhar A, Liggitt D, Krishnan KM. Chem Soc Rev. 2015; 44:8576–8607. [PubMed: 26390044]

29. Vasanawala SS, Nguyen KL, Hope MD, Bridges MD, Hope TA, Reeder SB, Bashir MR. Magn Reson Med. 2016; 75:2107–2111. [PubMed: 26890830]

30. Longmire M, Choyke PL, Kobayashi H. Nanomedicine. 2008; 3:703–717. [PubMed: 18817471]

31. Modo, M., Bulte, J. Molecular and Cellular MR Imaging. CRC Press; 2007.

32. Kuboyabu T, Yamawaki M, Aoki M, Ohki A, Murase K. Int J Nanomed Nanosurg. 2016; 2

33. Prabhakar U, Maeda H, Jain RK, Sevick-Muraca EM, Zamboni W, Farokhzad OC, Barry ST, Gabizon A, Grodzinski P, Blakey DC. Cancer Res. 2013; 73:2412–2417. [PubMed: 23423979]

34. Perry JL, Reuter KG, Kai MP, Herlihy KP, Jones SW, Luft JC, Napier M, Bear JE, DeSimone JM. Nano Lett. 2012; 12:5304–5310. [PubMed: 22920324]

35. Antonelli A, Sfara C, Battistelli S, Canonico B, Arcangeletti M, Manuali E, Salamida S, Papa S, Magnani M. PLoS One. 2013; 8:e78542. [PubMed: 24223101]

36. Steichen SD, Caldorera-Moore M, Peppas NA. Eur J Pharm Sci. 2013; 48:416–427. [PubMed: 23262059]

37. Swiercz R, Chiguru S, Tahmasbi A, Ramezani SM, Hao G, Challa DK, Lewis MA, Kulkarni PV, Sun X, Ober RJ, Mason RP, Ward ES. J Nucl Med. 2014; 55:1204–1207. [PubMed: 24868106]

38. Hong H, Yang Y, Zhang Y, Cai W. Curr Top Med Chem. 2010; 10:1237–1248. [PubMed: 20388105]

39. Bulte JWM, Walczak P, Gleich B, Weizenecker J, Markov DE, Aerts HCJ, Boeve H, Borgert J, Kuhn M. Proc SPIE Int Soc Opt Eng. 2011; 7965:79650z.

40. Bulte JWM, Walczak P, Janowski M, Krishnan KM, Arami H, Halkola A, Gleich B, Rahmer J. Tomography. 2015; 1:91–97. [PubMed: 26740972]

41. Hensley, D., Goodwill, P., Croft, L., Conolly, S. Preliminary experimental X-space color MPI. 2015 5th International Workshop on Magnetic Particle Imaging (IWMPI); 2015; p. 1-1.

42. Rahmer J, Halkola A, Gleich B, Schmale I, Borgert J. Phys Med Biol. 2015; 60:1775–1791. [PubMed: 25658130]

43. Mody VV, Cox A, Shah S, Singh A, Bevins W, Parihar H. Appl Nanosci. 2013; 4:385–392.

44. Bañobre López M, Teijeiro A, Rivas J. Rep Prac Oncol Radiother. 2013; 18:397–400.

45. Cole AJ, Yang VC, David AE. Trends Biotechnol. 2011; 29:323–332. [PubMed: 21489647]

46. Shi Q, Pisani LJ, Lee YK, Messing S, Ansari C, Bhaumik S, Lowery L, Lee BD, Meyer DE, Daldrup-Link HE. Contrast Media Mol Imaging. 2013; 8:281–288. [PubMed: 23606432]

47. Bauer LM, Situ SF, Griswold MA, Samia ACS. Nanoscale. 2016; 8:12162–12169. [PubMed: 27210742]

48. Hensley, D., Goodwill, PW., Dhavalikar, R., Tay, ZW., Zheng, B., Rinaldi, C., Conolly, SM. World Molecular Imaging Congress. 2016. A New Theranostics Platform: Magnetic Fluid Hyperthermia Localized with a Strong Gradient and Simultaneously Imaged with Magnetic Particle Imaging.
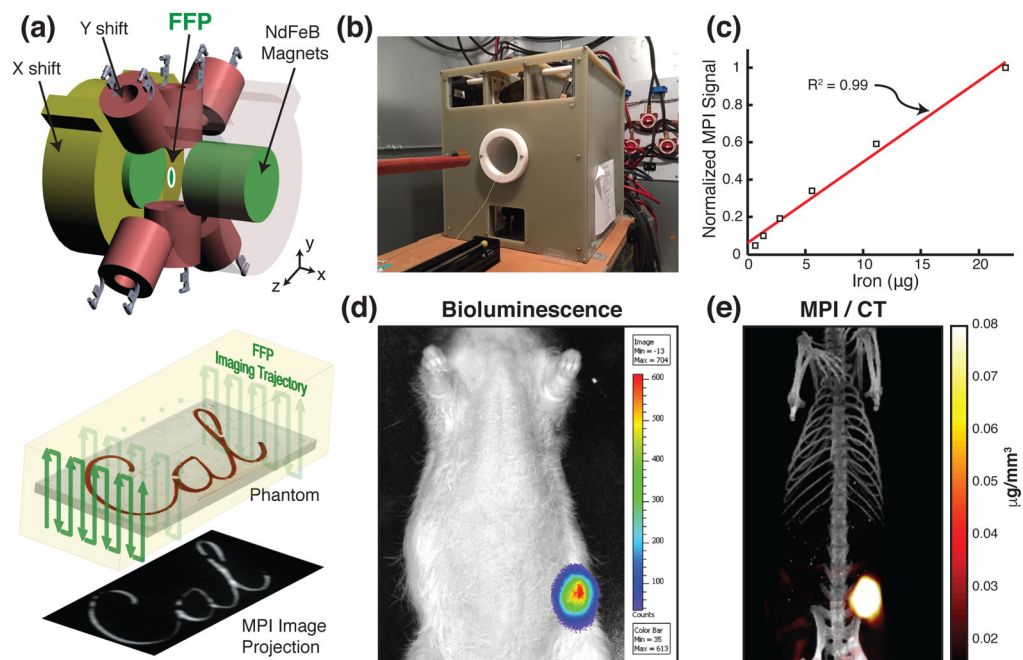
Figure 1.
(a) Illustration of Field Free Point (FFP) Magnetic Particle Imaging. A magnetic field gradient is created with NdFeB permanent magnets (green) and the FFP is shifted in x and y directions with electromagnets (yellow and red, respectively), and the animal bed is translated via a motor in the z direction. The FFP follows the specified trajectory through the sample in the FOV as shown, and a 3D MPI image is acquired. A maximum intensity projection of the 3D MPI image is shown. (b) Photograph of our custom-built FFP MPI scanner. (c) Plot of MPI signal from six samples of LS-008 particles from Lodespin Labs with concentrations ranging from 36 μg Fe/mL to 1.2 mg Fe/mL. SPIO signal in MPI is linear with SPIO concentration ($R^2 = 0.99$). (d) Representative bioluminescence image of the MDA-MD-231-luc xenograft tumor. (e) Corresponding maximum intensity projection of the 3D MPI image (shown FOV for lower abdomen: $4 \times 4 \times 5.8$ cm) acquired 6 hours after injection of long circulating LS-008 particles from Lodespin Labs with CT overlay.
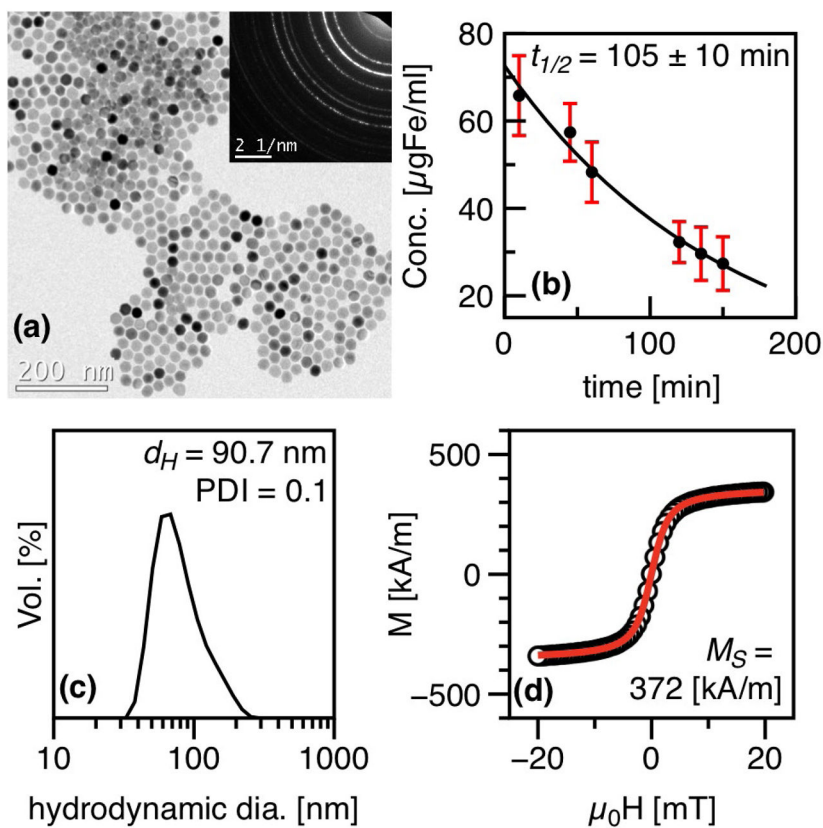
Figure 2.
(a) Bright field TEM image of uncoated iron oxide cores of LS-008 and (inset) Selected Area Diffraction pattern showing crystal morphology and characteristic spinel diffraction rings. (b) MPS signal intensity vs. time of blood samples taken from female CD-1 mice following tail vein injection of 5 mg Fe/kg. (c) Hydrodynamic size measured by DLS. (d) Magnetization curves measured by VSM at room temperature.
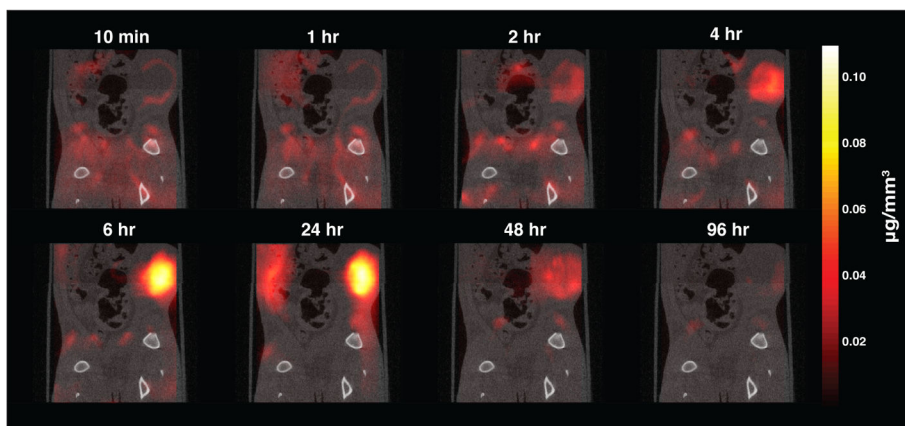
Figure 3.
Tracer Dynamics in Group A rats. Cropped FOV: 4 $\times$ 4 $\times$ 5.8 cm. Slices through the MPI volume over time are coregistered to corresponding CT slices and shown here. The exquisite contrast of MPI allows clear visualization of the dynamics: initial rim enhancement, followed by accumulation and then clearance.
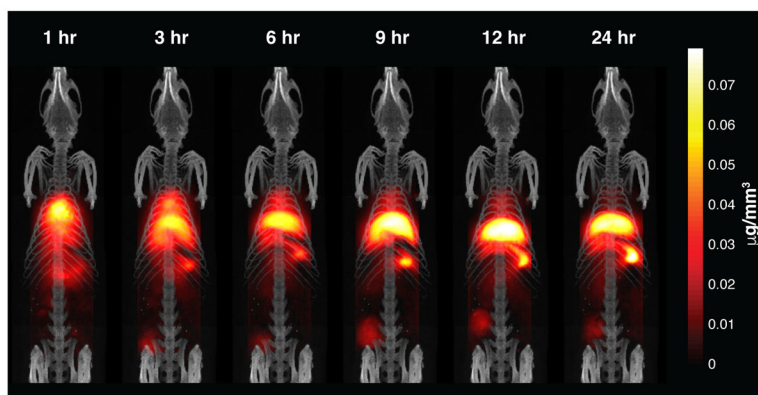
Figure 4.
Tracer Dynamics in Group B rats. Maximum intensity projection of 3D MPI volumes coregistered with a CT skeletal reference. The whole body tracer dynamics along with the tumor are clearly visualized.
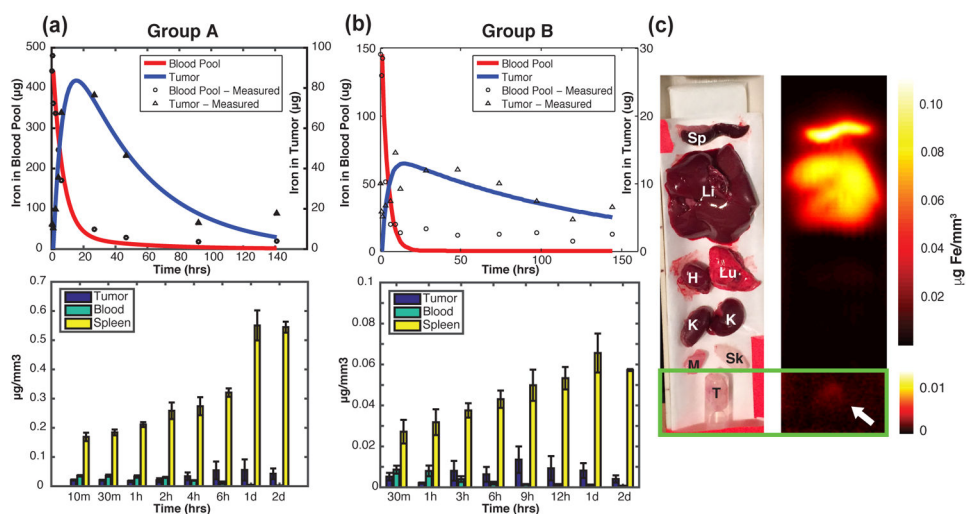
Figure 5.
(a) Group A two-compartment model fitting and biodistribution through time, n = 3. (b) Group B two-compartment model fitting and biodistribution through time, n = 3. (c) *ex vivo* MPI scan (right) and corresponding photograph (left) 2 days post SPIO injection.